JOURNAL OF GEOPHYSICAL RESEARCH, VOL. 105, NO. D11, PAGES 14,613–14,623, JUNE 16, 2000

Stratospheric ozone climatology from lidar measurements at Table Mountain (34.4°N, 117.7°W) and Mauna Loa (19.5°N, 155.6°W)

Thierry Leblanc and I. Stuart McDermid

Table Mountain Facility, Jet Propulsion Laboratory, California Institute of Technology, Wrightwood

Abstract. Using more than 1600 nighttime profiles obtained by the Jet Propulsion Laboratory differential absorption lidars located at Table Mountain Facility (TMF, 34.4°N) and Mauna Loa Observatory (MLO, 19.5°N) stratospheric ozone climatology is presented in this paper. These two systems have been providing high-resolution vertical profiles of ozone number density between 15 and 50 km for several nights a week since 1988 (TMF) and 1993 (MLO). The climatology presented here is typical of early night ozone values at both sites and typical of a low solar activity period for MLO. The observed seasonal and vertical structure of the ozone concentration at TMF is consistent with that typical of middle to subtropical latitudes. A clear annual cycle in opposite phases below and above the ozone concentration peak is observed. The observed winter maximum below the ozone peak is associated with a maximum day-to-day variability, typical of a dynamically driven lower stratosphere. The maximum concentration observed in summer above the ozone peak emphasizes the more dominant role of photochemistry. Unlike TMF, the ozone concentration observed at MLO tends to be higher during the summer months and lower during the winter months throughout the entire stratospheric ozone layer. Only a weak signature of the extratropical latitudes is observed near 19–20 km, with a secondary maximum in late winter. The only large variability observed at MLO is in the lowermost stratosphere, which could be associated with the natural variability of the tropical tropopause.

1. Introduction

For almost 2 decades now a large fraction of atmospheric science research has focused on ozone and more general climatic change issues. Since the discovery of the Antarctic ozone hole in the early 1980s [*Farman et al*., 1985], considerable progress has been made in the understanding of ozone depletion and its importance for the radiative balance of the atmosphere. However, large uncertainties remain, especially in the quantification of the more variable Arctic ozone hole and in the origin and magnitude of the recent ozone decline at high latitudes and midlatitudes [*Bojkov and Fioletov*, 1995, 1997]. Three main reasons are responsible for such uncertainties. First, the role of heterogeneous chemistry and polar stratospheric clouds (PSCs) [e.g., *Tolbert*, 1996] has only recently been assessed and still holds considerable quantitative and qualitative gaps. Second, the transport and mixing of ozone and other trace constituents from the tropics into the higher latitudes [*Brewer*, 1949] is still far from being understood and accurately quantified. Specific regional processes such as the tropical upwelling part of the Brewer-Dobson circulation [*Fahey et al*., 1996], the subtropical tropopause [*Holton et al*., 1995], and the polar vortex edge [*Schoeberl and Hartmann*, 1991] are still under intensive investigation. Also, the role of large-scale mixing, caused by polar vortex filaments at midlatitude, has recently been emphasized [*Orsolini*, 1995]. Third, because of the too coarse grids and/or inaccurate diffusivities used, numerical models are still unable to reproduce processes at small scales where mixing is believed to be crucial [e.g., *Edouard et al*., 1996].

It is therefore essential that a continuous and long-term global survey of the stratospheric ozone and its depleting substances be maintained. This is one of the main goals of the Network for Detection of Stratospheric Change (NDSC) [*Kurylo and Solomon*, 1990], a network of ground-based observation stations spread out around the globe. As part of the NDSC, two differential absorption lidars (DIALs) are operated by the Jet Propulsion Laboratory (JPL), one since 1988 at Table Mountain Facility, California (TMF, 34.4°N, 117.7°W), the other since 1993 at Mauna Loa Observatory, Hawaii (MLO, 19.5°N, 155.6°W). These two ozone DIAL systems provide high-resolution vertical profiles of ozone number density (15–50 km) and temperature (15–90 km). A temperature climatology at both of these NDSC sites has been recently published [*Leblanc et al*., 1998] and an earlier, pre-Pinatubo, 4-year ozone climatology has also been presented for TMF by *McDermid* [1993]. The updated 10-year ozone climatology at TMF and a new 6-year ozone climatology at MLO are presented in this paper. After a brief description of the instruments and data sets (section 2) the vertical and seasonal structure of nighttime ozone number density at both sites will be shown (section 3). These results will then be complemented with derived quantities such as the ozone column between the top of the profiles and 20 km altitude and the ozone mixing ratio (section 4).

2. Instruments and Data Sets

The ground-based DIAL method for measuring stratospheric profiles of ozone number density [*Schotland*, 1974;

Paper number 2000JD900030.

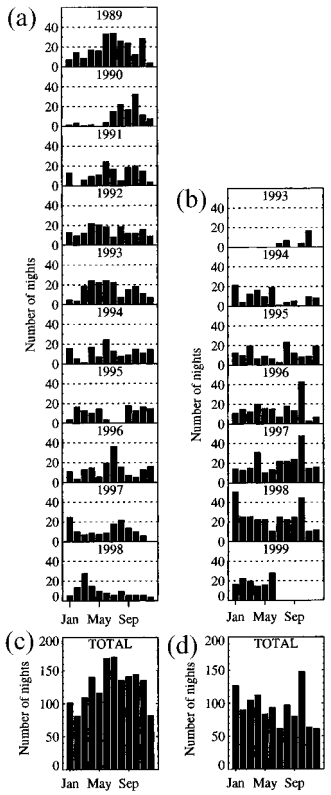

Figure 1. Monthly number of profiles (a) since 1989 at Table Mountain Facility (TMF) and (b) since 1993 at Mauna Loa Observatory (MLO) selected for this climatology and (c) the 1989–1998 (TMF) and (d) 1993–1999 (MLO) totals.

Mégie et al., 1977] has been commonly used in the past decade [e.g., *Pelon et al*., 1986; *McDermid et al*., 1990; *McGee et al*., 1991; *McGee et al*., 1997]. Laser radiation transmitted at two different wavelengths into the atmosphere is backscattered by molecules and particles in the atmosphere and collected by a telescope. In the DIAL method one wavelength is weakly absorbed by ozone (i.e., 308 nm), and the other is nonabsorbed (i.e., 353 nm). By comparing the vertical slope of the two returned signals the ozone number density can be deduced with a maximum precision near the ozone concentration peak (22–27 km). The method can utilize either Rayleigh scattering, when it is dominant compared to the aerosol scattering (i.e., at all times above ~30 km altitude and during volcanically quiescent periods in the lower atmosphere), or vibrational Raman scattering. The vibrational Raman signal is backscattered by nitrogen molecules, and the returned wavelengths are slightly shifted from the emitted wavelengths (i.e., 332 and 385 nm returned for 308 and 353 nm emitted, respectively).

Unlike the returned Rayleigh signal, the vibrational Raman signal is relatively insensitive to Mie scattering, making its use possible inside a potential stratospheric aerosol layer. Four receiving channels (all Rayleigh) are used in the JPL stratospheric DIAL system located at TMF [*McDermid et al*., 1990]. Six channels (four Rayleigh and two vibrational Raman) are used in a slightly improved system at MLO [*McDermid et al*., 1995a]. These two systems measure high-resolution profiles of nighttime ozone number density between 15 and 50 km. In the presence of strong aerosol loading, as, for example, after the Pinatubo eruption in 1991, the ozone can be measured at TMF only above the aerosol layer, which limits the bottom of the ozone profiles to altitudes of ~25–30 km.

The current instrumental vertical resolution for both systems is 300 m, but the TMF system was operated with a 600-m resolution until September 1994. During analysis the raw data are vertically filtered to reduce the instrumental noise. The resolution of the filter, the definition used to quantify the effect of filtering, is that commonly used for digital filters, i.e., equal to the inverse of the cutoff frequency of the filter. The vertical resolution is then equal to the smallest wavelength at which a vertical fluctuation has its amplitude halved after filtering. For the ozone profiles this resolution is almost 1 km near the ozone peak. It decreases to ~3 km at the bottom of the profiles and to 8–10 km at the top of the profiles.

For a typical experiment the minimum instrumental error, which occurs at the ozone peak, is a few percent. This error increases to 10–15% at the bottom of the profile (~15 km) and increases to more than 40% above 45 km because of the combined reduction in the returned signal and the lower ozone concentration at these altitudes. No results for altitudes above 45 km will be discussed in this paper. The overall performance of the MLO system is slightly better than that at TMF, leading to smaller errors at the top of the ozone profiles. The entire TMF and MLO data sets have been recently reanalyzed using new ozone/temperature analysis software (LidAna version 4.00 for future reference). This new software contains several improvements compared to the previous one, including enhanced signal saturation correction, background correction, vertical filtering, and use of combined channels.

The routine measurement modes for both lidars are based upon the NDSC requirement for a long-term ozone survey. The usual measurements comprise an ~1.5-hour- (MLO) or 2-hour (TMF)-long data acquisition at the beginning of the night several times a week, weather and instrument permitting (the normal starting time is the end of astronomical twilight, which ensures that there is no sunlight falling on any part of the atmosphere sensed by the lidar). Additional full night measurements have been made in the past 3 years at given periods of the year to study the tidal signature in middle atmospheric temperatures [*Leblanc et al*., 1999]. However, to avoid any contamination by possible diurnal variations, only the profiles taken before 0800 UT at TMF and before 0930 UT at MLO (i.e., 2400 LT for both stations) have been selected to build this climatology. The data set from the full night campaigns will be used in the future for the study of the ozone diurnal variations. This temporal selection leaves more than 850 early night ozone profiles between January 1, 1989, and December 31, 1998, at TMF and more than 800 profiles between July 1, 1993, and June 30, 1999, at MLO. The upper stratospheric results at MLO are expected to be slightly affected by the 11-year solar cycle since the 1993–1999 period of measurement is nearly centered on the 1996 solar minimum, thus covering the half cycle of lowest activity.

The number of profiles selected for this study is summarized in Figure 1. The density of measurements at MLO is higher than that at TMF because of better winter weather conditions and more full night campaigns. The large total number of profiles measured in October at MLO is due to the three full night campaigns held during at least 10 consecutive days in 1996, 1997, and 1998. Most of the time the first two profiles (i.e., ~3–4 hours) of each of these full nights have been selected, explaining the observed large total number of measurements that month. This disparity is not expected to contami-

nate significantly the climatological results since the minimum 40 profiles per month indicated already gives a good statistical base upon which to estimate the seasonal variability. The JPL lidars have participated in numerous intercomparison and validation exercises with nearly colocated and/or simultaneous measurements. The results of these campaigns have been extensively published and clearly indicate the quality of the lidar results [e.g., *McDermid et al*., 1995b, 1996; *Tsou et al*., 1995; *Planet et al*., 1995; *Baily et al*., 1996; *Bruhl et al*., 1996; *Froidevaux et al*., 1996; *Grant et al*., 1998; *McPeters et al*., 1999].

3. Results: Ozone Profiles

Figure 2 shows two typical ozone profiles measured at TMF in late winter and midsummer together with their respective $\pm 1\sigma$ measurement errors. As expected for midlatitudes, the ozone concentration peak is stronger and located lower in winter (5.5×10^{12} cm^{-3} at 23 km) than in summer (4.5×10^{12} cm^{-3} at 25–26 km). A thin strong peak (laminae) can be observed near 19–20 km. In March these laminae can sometime peak at $6-6.5 \times 10^{12}$ cm^{-3} around and below 20 km (not shown here).

Figure 3 is similar to Figure 2 but for two typical profiles measured at MLO. Unlike TMF, there are no significant seasonal changes in the altitude of the ozone peak (5×10^{12} cm^{-3} in summer and $4-4.2 \times 10^{12}$ cm^{-3} in winter near 24–26 km). Also unlike TMF, the ozone concentration in the lower stratosphere is not significantly higher in winter than in summer. Instead, the all-winter profile tends to have lower values than the summer profile. This is consistent with a more photochemically and/or radiatively driven tropical ozone abundance, where the role of transport and mixing by the midlatitude and high-latitude planetary waves is much less significant [*Randel et al*., 1993, and references therein]. Still, there remains in Figure 3 a layer in the winter lower stratosphere where ozone appears to be slightly more abundant than in summer. This feature

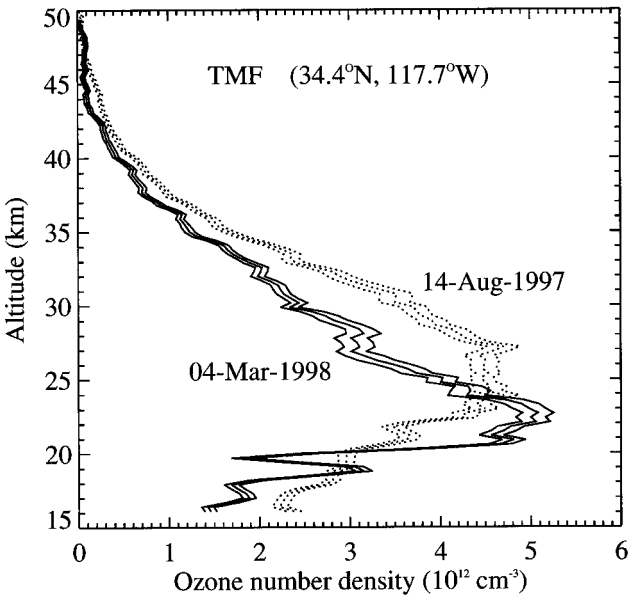

Figure 2. Two typical ozone profiles with their error bars (1σ), representative of wintertime and summertime, obtained by the differential absorption lidar (DIAL) ozone lidar at TMF.

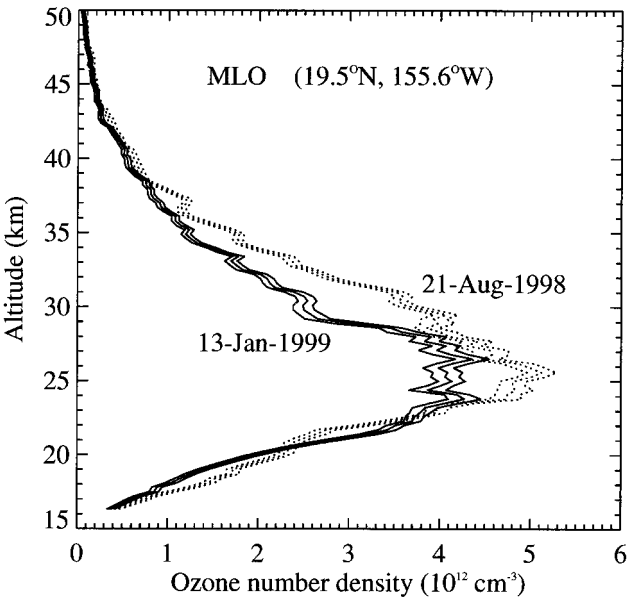

Figure 3. Same as Figure 2 but obtained by the DIAL ozone lidar at MLO.

mimics the ozone seasonal variability observed at TMF (Figure 2) at similar altitudes resulting from occasional winter midlatitude air mass intrusions (A. Hauchecorne, personal communication, 1999). This feature, however, does not prevail because of the day-to-day ozone variability and the instrumental errors.

All the selected ozone concentration profiles listed in Figure 1 have been interpolated to a 1-km vertical interval in order to homogenize the data set initially binned on either a 300 or 600 m instrumental grid. This operation reduces the magnitude of smaller vertical scale fluctuations, but these are not important for the climatological study presented in this paper. The 1989–1998 (TMF) overall mean ozone number density was calculated as a function of altitude. The mean profile obtained is representative of an annual mean since the data distribution for each month is nearly identical (see Figure 1). The deviations (in percent) from this quasi-annual mean have been plotted for each day of measurement in Figure 4 at four characteristic altitudes. The results are displayed in the form of a single composite year. The vertical bars indicate the 1σ errors (in percent) associated with each data point. The thick shaded line is the filtered data for each day of the composite year when at least one measurement has been performed that day of the year. The filter scheme, a second-order polynomial fitted over a 65-day wide window, takes into account the quality of each measurement. This way, less weight is given to shorter and/or noisier experiments with larger error bars. As anticipated from individual profiles (e.g., Figure 2), the seasonal variations below and above the ozone peak (~23 km) are inverted. At 30 and 44 km the maximum occurs in late summer, and the minimum occurs in winter, consistent with a radiatively driven ozone abundance. At 18 and 21 km the maximum occurs in late winter/early spring, and the minimum occurs in late summer, typical of a dynamically driven winter lower stratosphere, where polar and midlatitude relatively rich ozone air masses frequently intrude into subtropical latitudes such as that of Table Mountain (34.4°N). The magnitude of the winter peak to the summer peak variation is discussed later in this paper. The

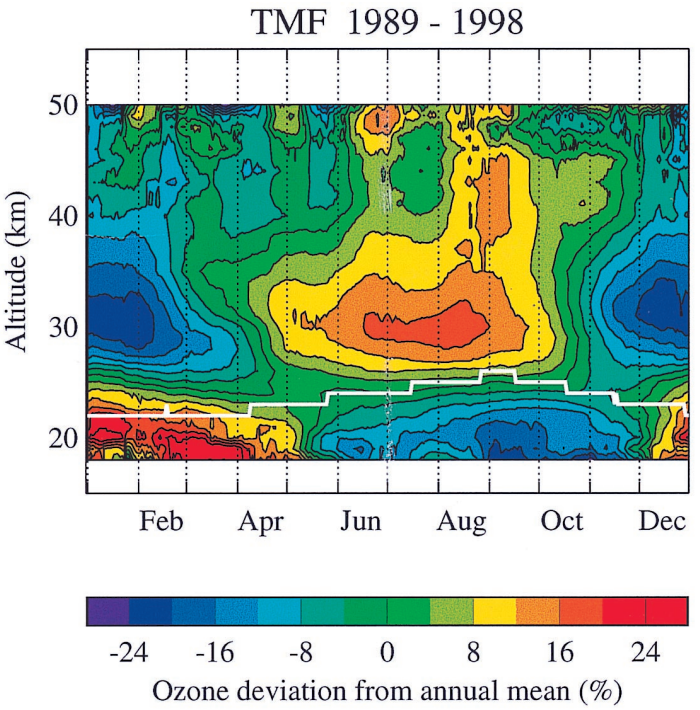

Plate 1. Ozone number density deviation from annual mean (in percent) at TMF (1989–1998 reduced to a single composite year) as a function of altitude and day of the year. The contour interval is 4%.

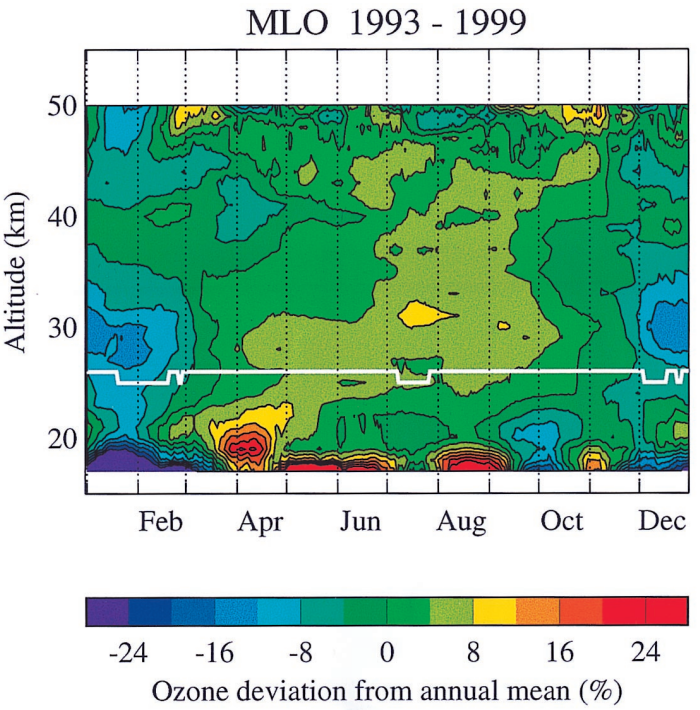

Plate 2. Same as Plate 1 but for the 1993–1999 period at MLO.

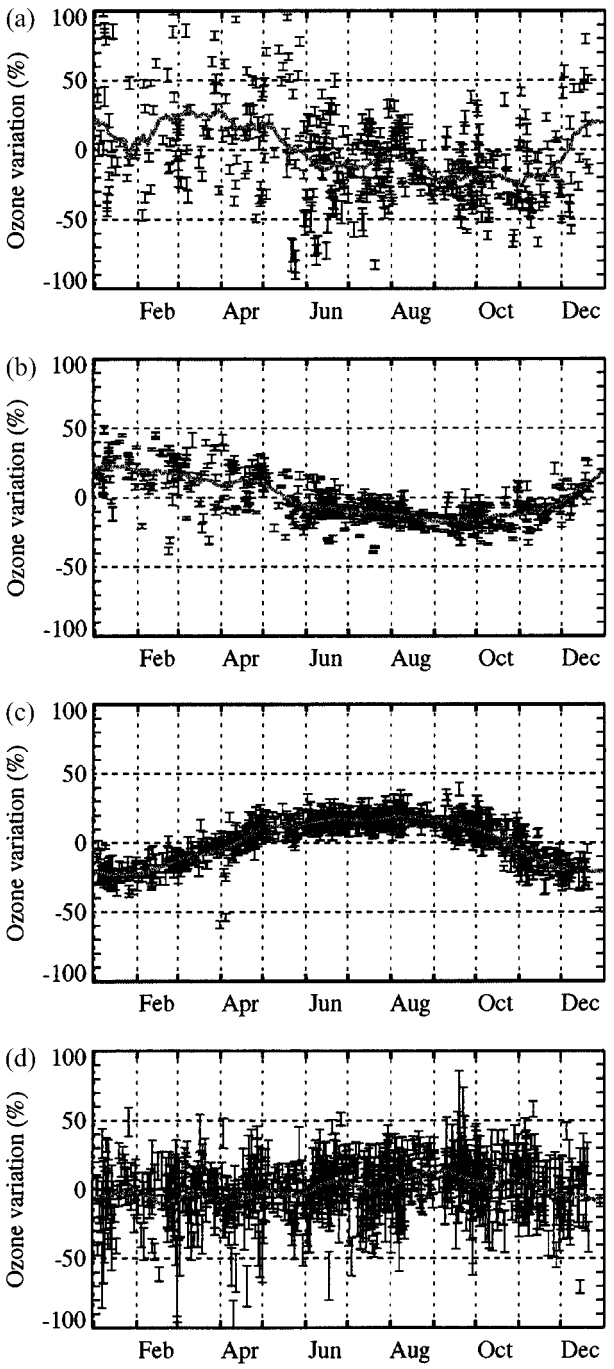

Figure 4. Seasonal variation (in percent) of stratospheric ozone number density at TMF (1989–1998 reduced to a single composite year) at four characteristic altitudes: (a) 18, (b) 21, (c) 30, and (d) 44 km. The vertical bars indicate the calculated total error at 1σ for each plotted measurement. The thick shaded line shows the 65-day filtered data (see text).

natural variability indicated by the magnitude of the deviations is much higher in the dynamically driven region (frequently as much as ±50% at 18 km). It is much weaker at 30 km, the region where the radiative effects are dominant. At 44 km the large error bars do not allow unequivocal conclusions, but the apparent low variability seems consistent with the observed low variability at 30 km.

Figure 5 is similar to Figure 4 but for the 1993–1999 period at MLO. The opposing characters of the ozone seasonal variation above and below the peak are not as clear as for TMF. There is no clear winter maximum at 21 and 18 km, nor is there a clear summer maximum at 30 and 44 km. Instead, at 30 km there is a plateau-like structure with higher concentrations during the entire summer and a short period of lower values in December and January. At 21 km, only a weak maximum is observed during late winter/early spring. However, the natural variability is significantly higher in winter (peaking at ±50%), emphasizing a residual influence of the northern midlatitude dynamics. At 18 km the variability is very high through all

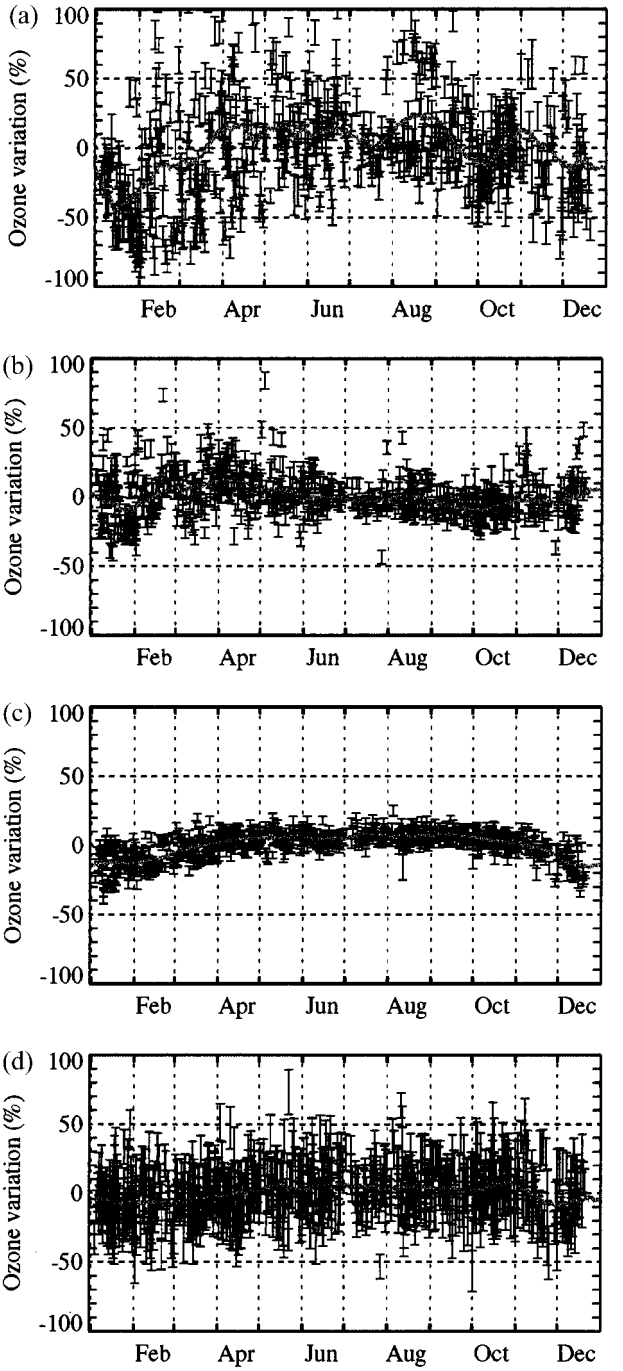

Figure 5. Same as Figure 4 but for the 1993–1999 period at MLO.

seasons. The high altitude and variability of the tropical tropopause height greatly influences total ozone and the ozone content of the lower stratosphere and is probably the cause of this observed high variability. Also, despite the low altitude of 18 km, Figure 5a exhibits relatively large error bars. This is due to the fact that unlike Figures 4a–4d and 5b–5d (and especially Figure 4a), the results displayed here come from the analysis of the vibrational Raman channels, which have lower signal-to-noise ratios. These large error bars are not observed for the other altitudes displayed since the Rayleigh channels are then used at ~20 km and above. To insure that the high variability observed at 18 km is not caused by some instrumental limitations, the results from the Rayleigh channels below 20 km were compared to those from the Raman channels. The data corrupted by aerosols, in particular after the Pinatubo eruption, have been removed from the Rayleigh data set. This way there is little or no contamination of the Rayleigh profiles by Mie scattering. The high natural variability observed in the Raman profiles of Figure 5a was also observed in the Rayleigh profiles (not shown). Thus it is confirmed that the observed high variability at 18 km is not the result of instrumental errors.

The filtered data plotted with thick shaded lines in Figures 4 and 5 were then contoured onto a two-dimensional (2-D) altitude/day-of-year grid. The 2-D contours of these filtered ozone deviations are shown in Plate 1 for the 1989–1998 period at TMF. The color scale extends from −24% (violet) to +24% (red), with a 4% contour interval. The white solid line near 22 km represents the averaged altitude of the ozone concentration peak. The seasonal variation of this altitude is well defined, with a maximum of 25 km in summer and a minimum of 22 km in winter. The pronounced seasonal variation of ozone concentration (in percent) is also clearly observed. The magnitude of the annual cycle above the ozone peak is maximum near 30 km with a peak-to-peak value exceeding 40%. At that altitude the maximum ozone concentration occurs in August while the minimum occurs in January. Above 30–35 km the annual cycle is not as clear despite a well-defined maximum in late August. Above 45 km the instrumental errors tend to hide the geophysical variability. Below the ozone concentration peak the relative magnitude of the annual cycle increases as we move downward. At 18 km (i.e., ~1 km above the tropopause in winter and ~2–3 km above the tropopause in summer) the peak-to-peak variation exceeds 45%, with the minimum occurring in September and the maximum occurring in March.

Plate 2 is similar to Plate 1 but for the 1993–1999 period at MLO. Again, the white solid line near 25 km represents the mean altitude of the ozone concentration peak. As noticed earlier in this paper, this altitude is almost the same throughout the entire year. Also, the seasonal variation of ozone concentration at MLO is not as pronounced as at TMF. Plate 2, nevertheless, highlights a residual annual cycle at 30 km and above similar to that observed at TMF and related to the seasonal variation of the radiative balance of the upper stratosphere (more sunlight in summer). The plateau-like structure observed at 30 km in Figure 5c is characterized here by a long summer season with ozone deviations between +4 and +8% (light green) surrounded by two short periods of transition from −12 to +4% (from blue to light green) and from +4 to −12% (from light green to blue). Plate 2 also shows a springtime maximum near 19–20 km, revealing a possible residual contamination by the midlatitude planetary wave activity. No clear annual cycle is observed below 25 km. However, despite the strong variability at the bottom of the profiles (near the tropopause), persistent high ozone concentrations are observed during the summer months, and persistent low concentrations are observed in December and January, indicating the dominant role of the photochemical and radiative effects over the dynamics. The annual cycles observed at both the TMF and MLO sites are in agreement to within a few percent with previous climatologies such as those performed by *Shiotani and Hasebe* [1994] using the Stratospheric Aerosol and Gas Experiment II (SAGE II) data.

For each altitude separately and for both TMF and MLO sites a weighted, two-component four-parameter sinusoidal fit has been applied to the measurements, similar to those plotted in Figures 4 and 5. The two constrained periods are 6 and 12 months. The results of the fits for TMF are plotted in Figure 6. Figure 6 (left) corresponds to the annual component, and Figure 6 (right) corresponds to the semiannual component. Figure 6 (top) is the amplitude (in percent), and Figure 6 (bottom) is the phase (i.e., time of maximum). The horizontal bars show the 1σ standard deviations returned for each parameter of the fit. Their magnitude depends on both the seasonal variations and the instrumental errors. As already observed on the 2-D contour plots, the annual phase inverts near 24 km from late winter in the lower stratosphere to late summer in the upper stratosphere (Figure 6 (left)). Except above 47 km and near 22 km, there is a quasi-absence of significant semiannual components. The semiannual amplitudes are weak, and the associated standard deviations are large. The only observed semiannual signature (near 20 km) appears to propagate downward with a phase propagation of ~3 km per month, but it remains weakly significant.

The results of the fits for MLO are given in Figure 7. The annual component is very well identified throughout the ozone layer (Figure 7 (left)). The annual phase is nearly constant (July then August above 35 km), except at 20 km, where it shifts to April. This shift is due to the residual early spring effect of the midlatitude intrusions already observed on the 2-D contours. As for TMF, there is a near-zero signature of the semiannual component. The semiannual amplitudes are weak, and the associated standard deviations are large.

4. Results: Derived Quantities

This section presents some results on quantities derived from the ozone concentration measurements presented in section 3. These quantities include the standard deviations from the monthly means, the integrated ozone columns, and the ozone mixing ratios.

To investigate the seasonal variation of ozone concentration variability, the standard deviation of the above profiles from the (composite) monthly means at each separate altitude has been calculated (in percent). The results are 2-D-contoured as a function of altitude and time of the year for TMF in Plate 3. Because of the increasing instrumental noise with height, the high variability observed above 45–47 km probably has little to do with natural variability. We will therefore not discuss any results above 45 km. Several distinctive regions can be observed. As was already observed in Figure 4 below 22 km, the maximum variability occurs in late winter/early spring, with

some standard deviations exceeding 30%. The variability is higher over a longer period (a half year) below 20 km, while it seems to be more concentrated in early spring between 20 and 23 km. Above the ozone concentration peak, two periods of higher variability are observed around 30 km altitude. These are the consequence of the seasonal transition from a winter to summer regime (spring maximum) and from a summer to winter regime (fall maximum). Also, the ozone variability appears to be higher in winter than in summer between 40 and 45 km altitude.

Plate 4 is similar to Plate 3 but for MLO. Again, very characteristic regions can be identified. Below the ozone peak the standard deviations from the monthly means reach 30–40% as they approach the tropical tropopause. The proximity of an upper and more variable winter tropopause [i.e., *Bojkov and Fioletov*, 1997] causes this variability to be higher in winter than in summer. Because of the close relationship between tropopause variability and lower stratospheric ozone variability [e.g., *Bodeker et al*., 1998], it is not possible to identify any signature other than the annual cycle. A deeper study of the relationship between tropopause height and lower stratospheric ozone would allow each component to be better isolated, but no tropopause information was available at the time this manuscript was written. The most remarkable feature observed above the ozone concentration peak is an apparent "double layer" of low variability surrounding a distinct maximum occurring in December-January near 30 km. The lower layer is located at the very same altitude as that of the ozone peak, and the upper layer is located between 35 and 40 km altitude.

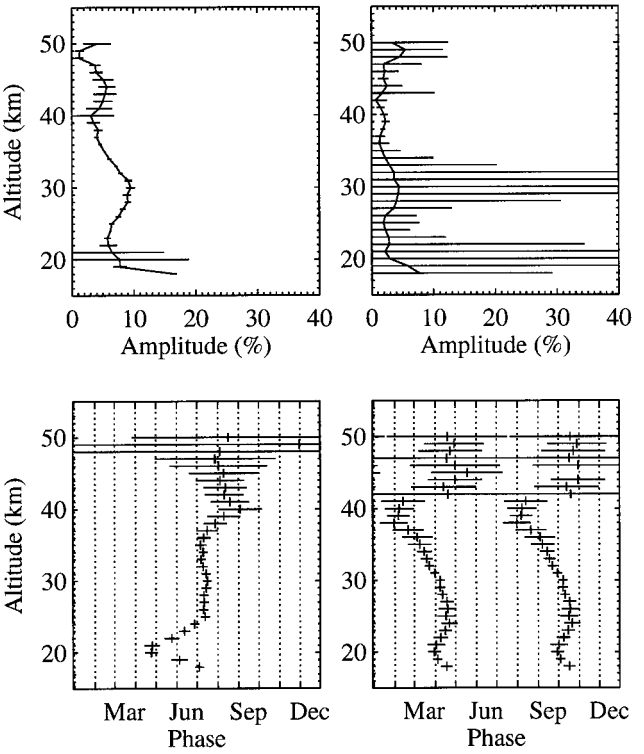

Figure 7. Same as Figure 6 but for the 1993–1999 period at MLO.

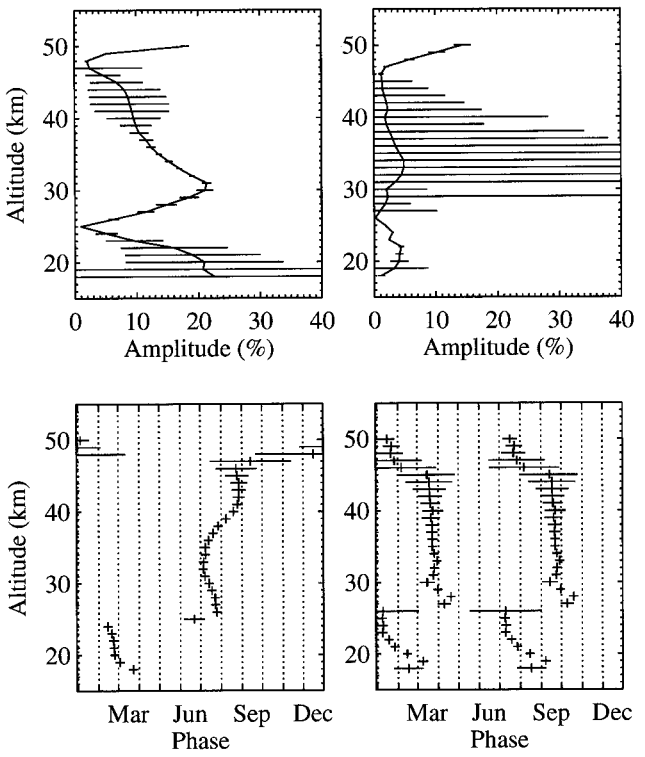

Figure 6. Ozone number density (right) annual and (left) semiannual (top) amplitudes and (bottom) phases calculated at TMF every 1 km from the 1989–1998 data plotted in Figure 3. The amplitudes are in percent of ozone change at each altitude.

Several tests have been performed to insure that this altitude dependency was not a consequence of the altitude-dependent data filtering nor due to the combined use of the Raman, Rayleigh-low, and Rayleigh-high channels. It appeared that even the use of the single Rayleigh-high channel led to the same results, which proves that vertical filtering and channel combination did not artificially cause this multilayer structure. This feature remains therefore unexplained at this time. Above 40 km a semiannual cycle with two maxima in winter and summer is observed, but the increasing instrumental noise reduces our confidence in this conclusion.

The ozone concentrations between the top of the profiles (50–55 km) and an altitude of 20 km are systematically integrated in the analysis process and converted to Dobson units (DU). The seasonal variation of these ozone columns for the period 1989–1998 at TMF is presented in Figure 8. As for Figures 4 and 5, the results are presented in the form of a composite year. A well-defined annual cycle is observed with a maximum of ~220 DU in summer and a minimum of 185 DU in winter. Although the ozone column does not include the lowest levels (15–20 km), the large winter variability is associated with the natural variability already observed in the vertical structure in the lower stratosphere. However, the annual cycle showing a maximum in summer is typical of the total ozone seasonal variations [*Bowman and Krueger*, 1985], suggesting that not too much information is lost by not including the lowermost stratospheric levels. Figure 9 is similar to Figure 8 but for the 1993–1999 period at MLO. Again, a clear annual variation is observed. This time, the summer maximum of 215 DU is observed during at least 5–6 months, from early April to early September, i.e., ~1 month longer than is observed at TMF. Then the ozone column drops at a near-constant rate of

8 DU per month, down to 180 DU in mid-January. It immediately increases again at a faster rate of 12 DU per month between mid-January and mid-April. These quick variations are associated with the maximum in the ozone concentration variability observed at 30 km in December/January in Plate 4.

For a convenient comparison with model results and other observations the ozone number densities measured by the two lidar systems have been converted into ozone mixing ratios. Since our measured densities are not absolute, and in order to insure hydrostaticity, the Mass Spectrometer Incoherent Scatter (MSIS)-90 [*Hedin*, 1991] empirically modeled air densities and temperatures [*Hedin*, 1991] have been used together to calculate the ozone mixing ratio as a function of pressure. Plate 5 and Plate 6 show the seasonal variations of the derived ozone mixing ratios for the periods 1989–1998 at TMF and 1993–1999 at MLO, respectively. Since the densities and temperatures (i.e., pressures) used do not come from actual simultaneous measurements, a slight vertical distortion of the contours is expected, especially during the winter months. This distortion can lead to some 10–15% differences in the regions of sharp vertical gradients, like in the late spring and summer lower stratosphere. The ozone mixing ratios at TMF located near 5 hPa in winter peak at ~6.5 ppmv, which is consistent with previous climatologies [e.g., *Fortuin and Kelder*, 1998]. In summer some differences, peaking at ±0.3 ppmv depending on the altitude, are observed for both sites, but these differences remain in the range of error caused by the use of an empirical model instead of simultaneous pressure and temperature measurements.

5. Conclusions

A 10-year and 6-year stratospheric ozone climatology obtained by the JPL DIAL instruments located at Table Mountain Facility (TMF, 34.4°N) and Mauna Loa Observatory (MLO, 19.5°N) respectively, have been presented in this paper. These two systems have been providing high-resolution vertical profiles of nighttime ozone number density between 15 and 50 km several nights a week since 1988 (TMF) and 1993 (MLO). The climatology presented is typical of early night ozone values and includes a negligible (MLO) to moderate (TMF) fraction of Pinatubo-influenced ozone values [*Parrish et al.*, 1998]. For MLO it includes ozone values typical of a time of low solar activity since the measurement period is approximately centered on the 1996 11-year solar cycle minimum.

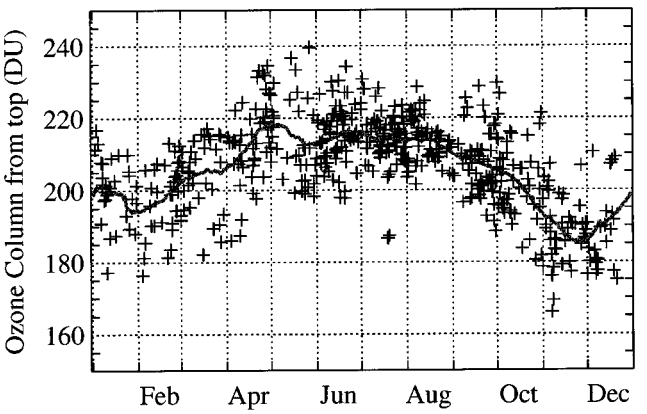

Figure 8. Seasonal variation (in Dobson units) of the ozone column between the top of the lidar profiles (~50–55 km) and 20 km altitude at TMF (1989–1998 reduced to a single composite year). The thick shaded solid line shows the 65-day filtered data (see text).

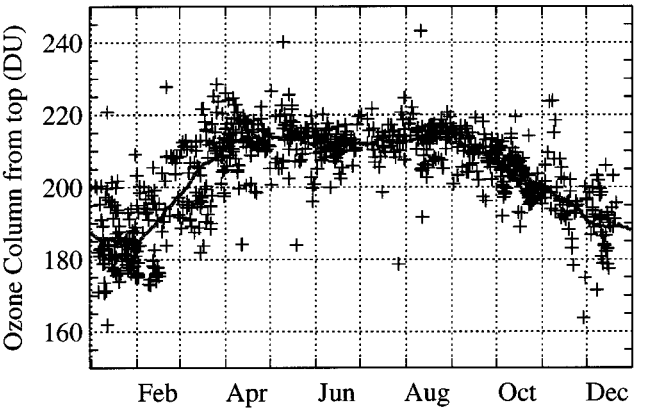

Figure 9. Same as Figure 8 but for the 1993–1999 period at MLO.

The observed seasonal and vertical structure of the ozone concentration at TMF is consistent with that typical of mid-latitude to subtropical latitudes [e.g., *Fortuin and Kelder*, 1998]. A clear annual cycle in opposing phases below and above the ozone concentration peak (~23 km) has been observed. The observed winter maximum below the ozone peak is associated with a maximum day-to-day variability, typical of a dynamically driven lower stratosphere. Ozone-rich air masses coming from the winter high latitudes frequently reach the latitude of TMF. Many polar air intrusions (A. Hauchecorne, personal communication, 1999) have been identified ("laminae"), especially at the end of the winter, accounting for a large fraction of the high ozone concentrations observed in this climatology below 21 km. The maximum ozone concentration observed in summer above the ozone peak emphasizes the more dominant role of photochemical and radiative effects in the upper stratosphere.

The seasonal and vertical structure of ozone has been investigated in a similar manner at MLO. Unlike TMF, the annual cycle does not show any opposing phases below and above the ozone peak. Instead, the ozone concentration tends to be higher during the summer months and lower during the winter months throughout the entire ozone layer. Only a weak signature of the extratropical latitudes is observed near 19–20 km, with a secondary ozone maximum in late March/early April. As emphasized above, the 1993–1999 measurement period at MLO is nearly centered on the 1996 11-year solar cycle minimum. Therefore the upper stratospheric ozone values are expected to be slightly lower (~2–3%) than those obtained over a full solar cycle [*Chandra and McPeters*, 1994].

The current climatology will be complemented by ongoing detailed investigations of the day-to-day variability involving ozone laminae (TMF), the tropopause variability (MLO and TMF), the diurnal variations, the interannual variability (quasi-biennial oscillation, El Nino and the Southern Oscillation, solar cycle, etc.), and the long-term trends of ozone at both sites. The results from these investigations, combined with the present climatology, will eventually provide a comprehensive overview of the stratospheric ozone vertical distribution above these two sites typical of subtropical and tropical latitudes.

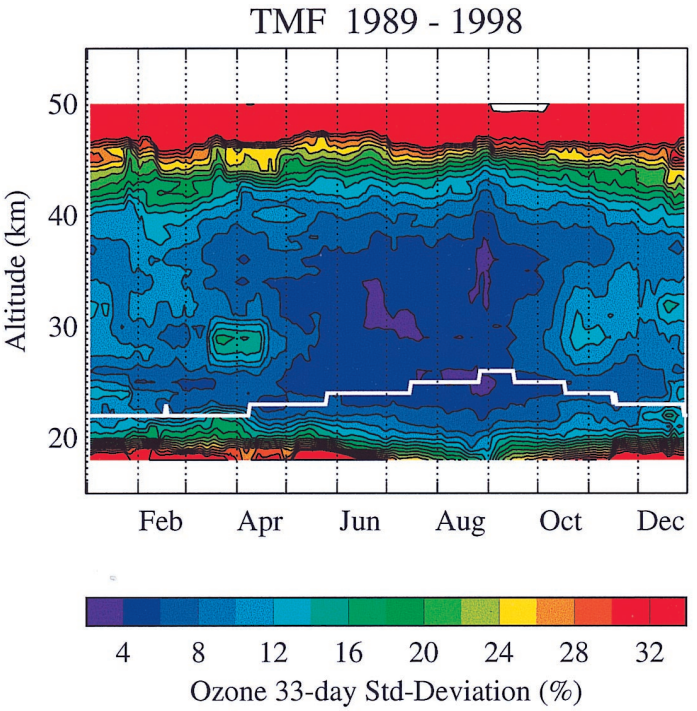

Plate 3. Ozone number density standard deviation from the 33-day mean (in percent) at TMF (1989–1998 reduced to a single composite year) as a function of altitude and day of the year. The contour interval is 2%.

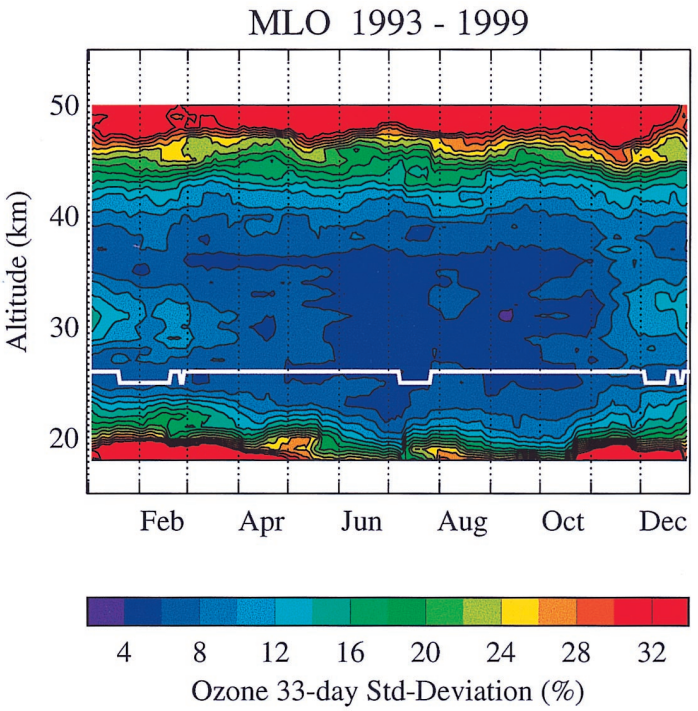

Plate 4. Same as Plate 3 but for the 1993–1999 period at MLO.

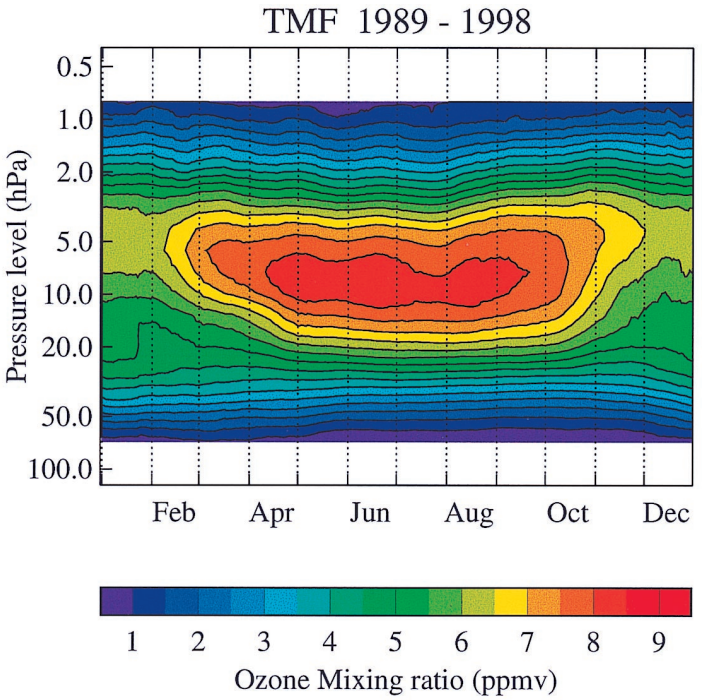

Plate 5. Ozone mixing ratio (in ppmv) derived using the ozone number density data contoured in Plate 1 (TMF 1989–1998) and the MSISE-90 empirical stratospheric density and temperature fields (see text). The contour interval is 0.5 ppmv.

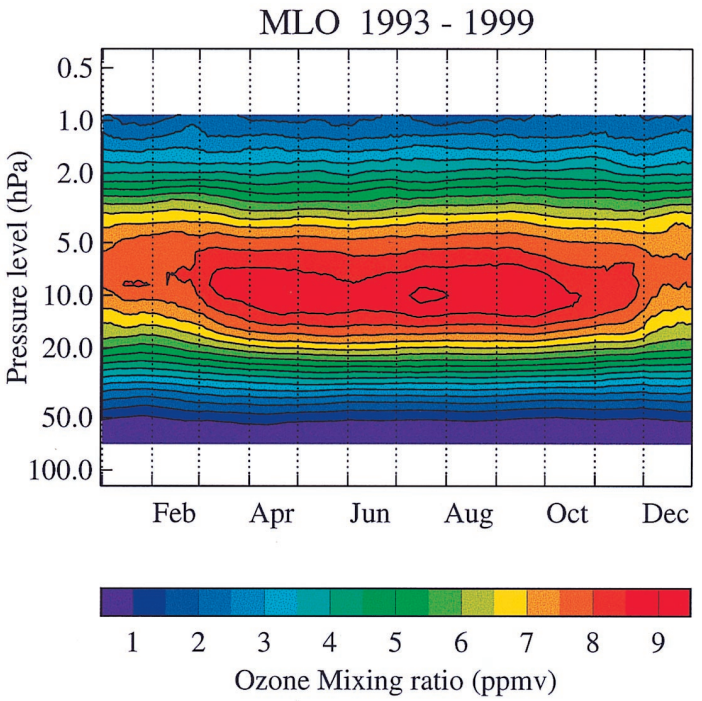

Plate 6. Same as Plate 5 but for the 1993–1999 period at MLO.

Acknowledgments. The work described in this paper was carried out at the Jet Propulsion Laboratory, California Institute of Technology, under an agreement with the National Aeronautics and Space Administration. The authors would like to thank those members of the JPL Lidar Team, T. Arakelian, G. Beyerle, R. P. Cageao, the late M. Schmoe, and T. D. Walsh, who assisted in the collection of the data used here.

References

Baily, P. L., et al., Comparison of cryogenic limb array etalon spectrometer (CLAES) ozone observations with correlative measurements, *J. Geophys. Res*., *101*, 9737–9756, 1996.

Bodeker, G. E., I. S. Boyd, and W. A. Matthews, Trends and variability in vertical ozone and temperature profiles measured by ozonesondes at Lauder, New Zealand: 1986–1996, *J. Geophys. Res*., *103*, 28,661–28,681, 1998.

Bojkov, R. D., and V. E. Fioletov, Estimating the global ozone characteristics during the last 30 years, *J. Geophys. Res*., *100*, 16,537–16,551, 1995.

Bojkov, R. D., and V. E. Fioletov, Changes of the lower stratospheric ozone over Europe and Canada, *J. Geophys. Res*., *102*, 1337–1347, 1997.

Bowman, K. P., and A. J. Krueger, A global climatology of total ozone from the Nimbus-7 Total Ozone Mapping Spectrometer (TOMS), *J. Geophys. Res*., *90*, 9767–9776, 1985.

Brewer, A. W., Evidence for a world circulation provided by the measurements of helium and water vapor distribution in the stratosphere, *Q. J. R. Meteorol. Soc*., *75*, 351–363, 1949.

Bruhl, C., S. R. Drayson, J. M. Russell, P. J. Crutzen, J. M. McInerney, P. N. Purcell, H. Claude, H. Gernandt, T. J. McGee, and I. S. McDermid, Halogen Occultation Experiment ozone channel validation, *J. Geophys. Res*., *101*, 10,217–10,240, 1996.

Chandra, S., and R. D. McPeters, The solar cycle variation of ozone in the stratosphere inferred from Nimbus 7 and NOAA 11 satellites, *J. Geophys. Res*., *99*, 20,665–20,671, 1994.

Edouard, S., B. Legras, F. Lefèvre, and R. Eymard, The effect of small-scale inhomogeneities on ozone depletion in the Arctic, *Nature*, *384*, 444–447, 1996.

Fahey, D. W., et al., In situ observation of NO_y, O_3, and the NO_y/O_3 ratio in the lower stratosphere, *Geophys. Res. Lett*., *23*, 1653–1656, 1996.

Farman, J. C., B. G. Gardiner, and J. D. Shanklin, Large losses of ozone in Antarctica reveal seasonal ClO_x/NO_x interaction, *Nature*, *315*, 207–210, 1985.

Fortuin, J. P. F., and H. Kelder, An ozone climatology based on ozonesonde and satellite measurements, *J. Geophys. Res*., *103*, 31,709–31,734, 1998.

Froidevaux, L., et al., Validation of UARS Microwave Limb Sounder ozone measurements, *J. Geophys. Res*., *101*, 10,017–10,060, 1996.

Grant, W. B., M. A. Fenn, E. V. Browell, T. J. McGee, U. N. Singh, M. R. Gross, I. S. McDermid, L. Froidevaux, and P.-H. Wang, Correlative stratospheric ozone measurements with the airborne UV DIAL system during TOTE/VOTE, *Geophys. Res. Lett*., *25*, 623–626, 1998.

Hedin, A. E., Extension of the MSIS thermosphere model into the middle and lower atmosphere, *J. Geophys. Res*., *96*, 1159–1172, 1991.

Holton, J. R., P. H. Haynes, M. E. McIntyre, A. R. Douglas, R. B. Rood, and L. Pfister, Stratosphere-troposphere exchange, *Rev. Geophys*., *33*, 403–439, 1995.

Kurylo, M. J., and S. Solomon, Network for the Detection of Stratospheric Change: A status and implementation report, NASA Upper Atmos. Res. Prog., Washington, D. C., 1990.

Leblanc, T., I. S. McDermid, P. Keckhut, A. Hauchecorne, C. Y. She, and D. A. Krueger, Temperature climatology of the middle atmosphere from long-term measurements at middle and low latitudes, *J. Geophys. Res*., *103*, 17,191–17,204, 1998.

Leblanc, T., I. S. McDermid, and D. A. Ortland, Lidar observations of the middle atmospheric thermal tides and comparison with the High Resolution Doppler Imager and Global Scale Wave Model, 1, Methodology and winter observations at Table Mountain (34.4°N), *J. Geophys. Res*., *104*, 11,917–11,929, 1999.

McDermid, I. S., A 4-year climatology of stratospheric ozone from lidar measurements at Table Mountain, 34.4°N, *J. Geophys. Res*., *98*, 10,509–10,515, 1993.

McDermid, I. S., S. M. Godin, and L. O. Lindqvist, Ground-based laser DIAL system for long-term measurements of stratospheric ozone, *Appl. Opt*., *29*, 3603–3612, 1990.

McDermid, I. S., T. D. Walsh, A. Deslis, and M. White, Optical systems design for a stratospheric lidar system, *Appl. Opt*., *34*, 6201–6210, 1995a.

McDermid, I. S., S. M. Godin, and T. D. Walsh, Results from the Jet Propulsion Laboratory stratospheric ozone lidar during STOIC 1989, *J. Geophys. Res*., *100*, 9263–9272, 1995b.

McDermid, I. S., T. J. McGee, and D. P. J. Swart, NDSC lidar intercomparisons and validation: OPAL and MLO3 campaigns in 1995, in *Advances in Atmospheric Remote Sensing With Lidar*, pp. 525–528, Springer-Verlag, New York, 1996.

McGee, T. J., D. Whiteman, R. Ferrare, J. J. Butler, and J. F. Burris, STROZ LITE: Stratospheric ozone lidar trailer experiment, *Opt. Eng*., *30*, 31–39, 1991.

McGee, T. J., M. Gross, U. Singh, P. Kimvilakani, A. Matthews, G. Bodeker, B. Conner, J. J. Tsou, M. Proffitt, and J. Margitan, Vertical profile measurements of ozone at Lauder, New Zealand during ASHOE/MAESA, *J. Geophys. Res*., *102*, 13,283–13,289, 1997.

McPeters, R. D., et al., Results from the 1995 Stratospheric Ozone Profile Intercomparison at Mauna Loa, *J. Geophys. Res*., *104*, 30,505–30,514, 1999.

Mégie, G., J. Y. Allain, M. L. Chanin, and J. E. Blamont, Vertical profile of stratospheric ozone by lidar sounding from the ground, *Nature*, *270*, 329–331, 1977.

Orsolini, Y. J., On the formation of ozone laminae at the edge of the Arctic polar vortex, *Q. J. R. Meteorol. Soc*., *121*, 1923–1941, 1995.

Parrish, A., B. J. Connor, J. J. Tsou, G. Beyerle, I. S. McDermid, and S. M. Hollandsworth, Microwave ozone and lidar aerosol profile observations at Table Mountain, California, following the Pinatubo eruption, *J. Geophys. Res*., *103*, 22,201–22,208, 1998.

Pelon, J., S. Godin, and G. Mégie, Upper stratospheric (30–50 km) lidar observations of the ozone vertical distribution, *J. Geophys. Res*., *91*, 8667–8671, 1986.

Planet, W. G., A. J. Miller, J. J. DeLuisi, D. J. Hofmann, S. J. Oltmans, J. D. Wild, I. S. McDermid, R. D. McPeters, and B. J. Connor, Comparison of NOAA-11 SBUV/2 Ozone Vertical Profiles with Correlative Measurements, *Geophys. Res. Lett*., *23*, 293–296, 1995.

Randel, W. J., J. C. Gille, A. E. Roche, J. B. Kumer, J. L. Mergenthaler, J. W. Waters, E. F. Fishbein, and W. A. Lahoz, Stratospheric transport from the tropics to middle latitudes by planetary-wave mixing, *Nature*, *365*, 533–535, 1993.

Schoeberl, M. R., and D. L. Hartmann, The dynamics of the stratospheric polar vortex and its relation to springtime ozone depletion, *Science*, *251*, 46–52, 1991.

Schotland, R. M., Errors in the lidar measurements of atmospheric gases by differential absorption, *J. Appl. Meteorol*., *13*, 71–78, 1974.

Shiotani, M., and F. Hasebe, Stratospheric ozone variations in the equatorial region as seen in Stratospheric Aerosol and Gas Experiment data, *J. Geophys. Res*., *99*, 14,564–14,584, 1994.

Tolbert, M. A., Update: Polar clouds and sulfate aerosols, *Science*, *272*, 1597–1597, 1996.

Tsou, J. J., B. J. Connor, A. Parrish, I. S. McDermid, and W. P. Chu, Ground-based microwave monitoring of middle atmosphere ozone: Comparison to lidar and Stratospheric and Gas Experiment II satellite-observations, *J. Geophys. Res*., *100*, 3005–3016, 1995.

T. Leblanc and I. S. McDermid, Table Mountain Facility, Jet Propulsion Laboratory, California Institute of Technology, P.O. Box 367, Wrightwood, CA 92397-0367. (leblanc@tmf.jpl.nasa.gov).

(Received August 17, 1999; revised November 30, 1999; accepted December 6, 1999.)